


Relativistic-coupled-cluster-theory analysis of properties of Co-like ions

Dillip K. Nandy^{1,*} and B. K. Sahoo^{2,†}

¹*Center for Theoretical Physics of Complex Systems, Institute for Basic Science (IBS), Daejeon 34126, Korea*

²*Atomic, Molecular and Optical Physics Division, Physical Research Laboratory, Ahmedabad-380009, India*

 (Received 24 August 2021; revised 1 November 2021; accepted 3 November 2021; published 19 November 2021)

Ionization potentials, excitation energies, transition properties, and hyperfine structure constants of the low-lying $3p^63d^9\ ^2D_{5/2}$, $3p^63d^9\ ^2D_{3/2}$, $3p^53d^{10}\ ^2P_{3/2}$, and $3p^53d^{10}\ ^2P_{1/2}$ atomic states of the Co-like highly charged ions such as Y^{12+} , Zr^{13+} , Nb^{14+} , Mo^{15+} , Tc^{16+} , Ru^{17+} , Rh^{18+} , Pd^{19+} , Ag^{20+} , and Cd^{21+} are investigated. The singles and doubles approximated relativistic coupled-cluster theory in the framework of one electron removal Fock-space formalism is employed over the Dirac-Hartree-Fock calculations to account for the electron correlation effects for determining the aforementioned properties. Higher-order relativistic corrections due to the Breit interaction and quantum electrodynamics effects in the evaluation of energies are also quantified explicitly. Our estimated values are compared with the other available theoretical calculations and experimental results, which are found to be in good agreement with each other.

DOI: [10.1103/PhysRevA.104.052812](https://doi.org/10.1103/PhysRevA.104.052812)

I. INTRODUCTION

The spectroscopic study of highly charged ions (HCIs) of heavy and moderately heavy elements has been the subject of primary interest in many contemporary areas of theoretical and experimental research fields. This includes tokamak plasmas and other high-temperature-plasma devices [1,2], electron-beam ion trap (EBIT) [3–9], stellarators [10], atomic clocks [11–15], and probing fundamental physics [15–18]. One of the important implications of these HCIs is the use of their forbidden transition lines in plasma diagnostics. For example, various visible or ultraviolet magnetic-dipole ($M1$) transition lines of Ti-like ions were analyzed for density diagnostics in hot plasmas since the pioneering work of Feldman *et al.* [19]. Furthermore, accurate measurements of wavelengths, excitation energies and other spectroscopic properties of these ions also drive various theoretical research areas of the HCIs; especially in analyzing the astrophysical and laboratory plasma. Besides the plasma diagnostics, high-precision calculations of different radiative properties of the HCIs play an important role in testing several *ab initio* theories of quantum many-body systems where the relativistic and bound quantum electrodynamic (QED) effects play crucial roles in explaining the experimental predictions. This is why both the forbidden and allowed transition properties of various HCIs have been investigated in many earlier studies by employing various relativistic methods (e.g., see Refs. [11,15,16,20–25]).

In the present study, we have investigated various transition properties of the highly charged Co-like transition-metal ions such as Y^{12+} , Zr^{13+} , Nb^{14+} , Mo^{15+} , Tc^{16+} , Ru^{17+} , Rh^{18+} , Pd^{19+} , Ag^{20+} , and Cd^{21+} . In particular, we have calculated the

first four low-lying atomic states of these ions in the framework of four-component relativistic coupled-cluster (RCC) theory. The four low-lying states include the $3p^63d^9\ ^2D_{5/2}$, $3p^63d^9\ ^2D_{3/2}$, $3p^53d^{10}\ ^2P_{3/2}$, and $3p^53d^{10}\ ^2P_{1/2}$ states, which are in fact one electron less than the $[3p^63d^{10}]$ closed-shell configuration; i.e., from the ground-state configuration of the Ni isoelectronic sequence ions. Thus, it is convenient to adopt a Fock-space approach to determine the wave functions of the above states by starting calculations for the $[3p^63d^{10}]$ configuration.

On the experimental interest of the Co-like ions, there are already a few observations available for several Co-like ions. For instance, Suckewer *et al.* identified the $M1$ transition lines between the fine-structure splitting of the ground-state configuration of the Co-like Mo and Zr ions in the Princeton Large Torus tokamak plasma [26]. Similarly, prior identified forbidden transitions of Nb^{14+} in the emission lines from the intense, continuous beams of metastable HCIs produced by an electron cyclotron resonance ion source [27]. There are also a few experimental identifications of lines available for the allowed $3p^63d^9\ ^2D_{5/2,3/2} \rightarrow 3p^53d^{10}\ ^2P_{1/2,3/2}$ transitions. Edlén first observed the allowed $3p^63d^9 \rightarrow 3p^53d^{10}$ transitions in the Sr^{11+} , Y^{12+} , Zr^{13+} , and Mo^{15+} HCIs in the spectra of hot tokamak plasmas along with other isoelectronic series of ions. Although, his observation did not yield any direct measurements of wavelengths for the Co-like ions as clearly made for the other isoelectronic series, however, it provided significant useful information in identifying the allowed transition lines [28]. Ekberg *et al.* observed various electric-dipole ($E1$) transitions such as the $3p^53d^{10}\ ^2P_{3/2} \rightarrow 3p^63d^9\ ^2D_{3/2}$, $3p^53d^{10}\ ^2P_{3/2} \rightarrow 3p^63d^9\ ^2D_{5/2}$, and $3p^53d^{10}\ ^2P_{1/2} \rightarrow 3p^63d^9\ ^2D_{3/2}$ transitions in Ru^{17+} , Rh^{18+} , Pd^{19+} , Ag^{20+} , and Cd^{21+} along with several other Co-like ions [29]. Alexander *et al.* also reported measurements of these allowed transitions among the ground-state and first-excited-state doublets of the Y^{12+} - Mo^{15+} ions [30]. In another experiment, Burkhalter *et al.* observed the spectra of the Co-like Sr^{11+} , Y^{12+} , Zr^{13+} , Nb^{14+} , and Mo^{15+} ions

*nandy@ibs.re.kr

†bijaya@prl.res.in

by employing a low inductance vacuum spark and a 10.7-m grazing-incidence spectrograph in the region 40–95 Å [31].

There are also a few theoretical calculations available on a number of Co-like ions but focusing mainly on the ground-state fine-structure splitting. For example, Guo *et al.* calculated the $3p^6 3d^9 \ ^2D_{5/2}$ and $3p^6 3d^9 \ ^2D_{3/2}$ states using the multiconfiguration-Dirac-Hartree-Fock (MCDHF) and relativistic many-body perturbation theory (RMBPT) [32]. They also estimated other transition properties involving these two states from their calculations. Their results show that values from the MCDHF method provides relatively more accurate calculations than those obtained using the RMBPT method. In another study, Chen *et al.* used an older version of the MCDHF code by Grant *et al.* [33] for determining the wavelengths of the fine-structure splitting of the ground-state configuration in Zr^{13+} , Nb^{14+} , and Mo^{15+} , which predicted larger values for the wavelengths than were obtained using the MCDHF and RMBPT methods [32]. Since the truncated RCC theory includes electron correlation effects to all-orders over the finite-order RMBPT method and take care of the size-inconsistency issue over the approximated MCDHF method, the calculations employing the RCC methods are believed to offer more reliable results for the transition properties of the investigated Co-like ions. Moreover, we have accounted for contributions from the leading-order QED corrections and the Breit interaction effects mediated by the transverse component of the virtual photon between the electrons that are typically significant in the HCIs.

The present paper is organized as follows: In Sec. II, we briefly describe the approximations made in the Hamiltonian to include various physical effects within the atomic systems and the mean-field method considered as the initial approximation to generate the single-particle atomic orbitals. In Sec. III, we discuss about the Fock-space based RCC theory that is employed to determine the energies and transition matrix elements of the aforementioned states of the Co-like HCIs. Then, we present the formulas used to estimate the transition probabilities, lifetimes, and hyperfine structure constants of the atomic states in Sec. IV. In Sec. V, we present the results and discuss them in comparison with the previously reported values before concluding the work. Unless stated otherwise, all the quantities are given in atomic units (a.u.).

II. APPROXIMATIONS IN ATOMIC HAMILTONIAN

The general relativistic many-body Hamiltonian that incorporates the usual longitudinal component of the Coulomb interactions between the electrons in an atomic system is given by

$$H_{DC} = \sum_i^N \left[c\boldsymbol{\alpha}_i \cdot \mathbf{p}_i + (\beta_i - 1)c^2 + V_{nuc}(r_i) + \sum_{j>i} V_C(r_{ij}) \right]. \quad (1)$$

Here, the subscript ‘‘DC’’ refers to the short-hand notation for the Dirac-Coulomb Hamiltonian, the first term describes the kinetic-energy part of the electrons, the second term denotes the rescaling of atomic Hamiltonian by subtracting the rest-mass energy of the electron, third term $V_{nuc}(r_i)$ is the nuclear potential with a Fermi-type charge distribution, and the last

term is the two-body Coulomb repulsion term between the electrons. N is the total number of the electron in the system and $\boldsymbol{\alpha}_i$ and β_i are the usual 4×4 Dirac matrices.

Since the considered systems are highly charged, so the relativistic effects in these ions are anticipated to be quite large. Therefore, for the accurate calculations of excitation spectra and transitions properties, it is necessary to incorporate higher-order relativistic effects at the one-body and two-body levels. At the two-body level, higher-order relativistic effects are accounted through the Breit-interactions mediated by the exchange of the transverse component of the virtual photon between the electrons and have the form [35]

$$V_{Br}(r_{ij}) = -\frac{1}{2r_{ij}} \{ \boldsymbol{\alpha}_i \cdot \boldsymbol{\alpha}_j + (\boldsymbol{\alpha}_i \cdot \hat{\mathbf{r}}_{ij})(\boldsymbol{\alpha}_j \cdot \hat{\mathbf{r}}_{ij}) \}, \quad (2)$$

where $r_{ij} = |\vec{r}_i - \vec{r}_j|$ denotes the absolute magnitude of the difference between radial vectors of any two electrons at positions \vec{r}_i and \vec{r}_j . Similarly, the higher-order relativistic effects that occur between the electrons and the nucleus is taken into the nuclear potential energy by defining effective model potentials. This includes leading-order vacuum-polarization (VP) and self-energy (SE) effects. In our calculation, the net effective QED potential of an electron at the position r_i is expressed as

$$V_{nuc}^{QED}(r_i) = V_{Uhl}(r_i) + \frac{2}{3}V_{WK}^{simple}(r_i) + V_{mf}(r_i) + V_{ef}(r_i). \quad (3)$$

The first two terms $V_{Uhl}(r_i)$ and $V_{WK}^{simple}(r_i)$ are known as the Uehling and Wichmann-Kroll model potentials arising due to the VP effects on the bound electrons. Similarly, the last two terms $V_{mf}(r_i)$ and $V_{ef}(r_i)$ represent the magnetic and electric form factors arising due to the SE corrections to the bound electrons. Analytical expressions for these $V_{Uhl}(r_i)$, $V_{WK}^{simple}(r_i)$, $V_{mf}(r_i)$, and $V_{ef}(r_i)$ terms are given by [12,36]

$$V_{Uhl}(r) = -\frac{4\alpha^2}{9r} V_{fermi}(r) \times \int_1^\infty dt \sqrt{t^2 - 1} \left(\frac{1}{t^2} + \frac{1}{2t^4} \right) e^{-2rt/\alpha}, \quad (4)$$

$$V_{WK}^{simple}(r) = -\frac{2}{3} \frac{\alpha}{\pi} V_{fermi}(r) \frac{0.092Z^2/\alpha^2}{1 + (1.62r/\alpha)^4}, \quad (5)$$

$$V_{mf}(r) = \frac{\alpha^2}{4\pi} i\vec{\gamma} \cdot \vec{\nabla} \left[V_{fermi}(r) \left(\int_1^\infty dt \frac{1}{\sqrt{t^2 - 1}} e^{-2tr/\alpha} \right) \right], \quad (6)$$

and

$$V_{ef}(r) = -A(Z, r) \frac{\alpha}{\pi} V_{fermi}(r) \int_1^\infty dt \frac{e^{-2tr/\alpha}}{\sqrt{t^2 - 1}} \left[\left(1 - \frac{1}{2t^2} \right) \times \{ \ln(t^2 - 1) + 4 \ln(1/Z\alpha + 0.5) \} - \frac{3}{2} + \frac{1}{t^2} \right] \times B(Z)Z^4 \alpha^3 e^{-Zr}, \quad (7)$$

where the factors $A(Z, r) = \{1.071 - 1.97[(Z - 80)\alpha]^2 - 2.128[(Z - 80)\alpha]^3 + 0.169[(Z - 80)\alpha]^4\}(r/\alpha)(r/\alpha + 0.07Z^2\alpha^2)$ and $B(Z) = 0.074 + 0.35Z\alpha$.

Thus, the final Hamiltonian that has been used in the present calculation has the following form:

$$H_{\text{DCBVS}} = H_{\text{DC}} + \sum_i^N \left[V_{\text{nuc}}^{\text{QED}}(r_i) + \sum_{j>i} V_{\text{Bre}}(r_{ij}) \right]. \quad (8)$$

The exact solution of the above Hamiltonian is not possible due to the two-body interaction terms (Coulomb and Breit), so one of the practical approaches to tackle the many-body problem is to start with a mean-field approximation. In the present work, we use the relativistic Hartree-Fock (HF) or Dirac-Hartree-Fock (DHF) method to obtain the mean-field wave function $|\Phi_0\rangle$ of the $[3p^6 3d^{10}]$ closed-shell configuration, its detailed underlying theory can be found elsewhere [37–39], to obtain the single-particle orbitals of the considered atomic systems.

To carry out the calculations conveniently, we define the normal order form of the atomic Hamiltonian defined with respect to the (D)HF wave function $|\Phi_0\rangle$ (reference state) of the $[3p^6 3d^{10}]$ closed-shell configuration, in this case by defining

$$\begin{aligned} H_N &= H_{\text{DCBVS}} - \langle \Phi_0 | H_{\text{DCBVS}} | \Phi_0 \rangle \\ &= H_{\text{DCBVS}} - E_{\text{SCF}}, \end{aligned} \quad (9)$$

with the self-consistent-field (SCF) energy E_{SCF} . Then, we employ the Fock-space approach to obtain the atomic wave functions of the $3p^6 3d^9 2D_{5/2}$, $3p^6 3d^9 2D_{3/2}$, $3p^5 3d^{10} 2P_{3/2}$, and $3p^5 3d^{10} 2P_{1/2}$ states of the Co-like ions.

III. RELATIVISTIC COUPLED-CLUSTER METHOD FOR ONE-ELECTRON DETACHMENT

As mentioned earlier, the atomic states that are being investigated in the reported HCIs are the four low-lying states of the Co isoelectronic series, which are the $3p^6 3d^9 2D_{5/2}$, $3p^6 3d^9 2D_{3/2}$, $3p^5 3d^{10} 2P_{3/2}$, $3p^5 3d^{10} 2P_{1/2}$ states, and their configurations are one electron short of the closed-shell configuration $[3p^6 3d^{10}]$. We consider here single-referee RCC theory in the similar philosophy of the electron detachment approach as discussed in Refs. [37,40] to obtain the wave functions of the above states. The basic strategy of this approach is described briefly as follows: After obtaining the DHF wave function $|\Phi_0\rangle$ of the $[3p^6 3d^{10}]$ closed-shell configuration, we determine its exact wave function using the RCC theory ansatz [37,40]

$$|\Psi_0\rangle = e^T |\Phi_0\rangle, \quad (10)$$

where T is defined as the linear combinations of all possible hole-particle excitation operators that are responsible for accounting for the neglected residual interactions in the calculation of the DHF wave function. The amplitudes of these operators are obtained by solving the nonlinear equation [37,40,41]

$$\langle \Phi_0^* | \widehat{H_N e^T} | \Phi_0 \rangle = 0, \quad (11)$$

where $|\Phi_0^*\rangle$ represents the excited Slater determinants with respect to $|\Phi_0\rangle$. After obtaining the RCC amplitudes, the exact energy of the $[3p^6 3d^{10}]$ configuration is obtained by

$$E_0 = E_{\text{SCF}} + \langle \Phi_0 | H_N | \Phi_0 \rangle. \quad (12)$$

In the Fock-space approach of RCC theory, we define a new working reference state $|\Phi_a\rangle = a_a |\Phi_0\rangle$, with a_a representing annihilation operator for an electron in the core orbital a to obtain the desired reference states of interest. Then, the exact atomic states are obtained by expressing [11,22]

$$\begin{aligned} |\Psi_a\rangle &= a_a |\Psi_0\rangle + R_a a_a |\Psi_0\rangle \\ &= \{1 + R_a\} e^T |\Phi_a\rangle, \end{aligned} \quad (13)$$

where R_a denotes additional RCC operator that is introduced to remove the extra electron correlation effects incorporated in the determination of $|\Psi_0\rangle$ due to the core electron a to give rise to $|\Psi_a\rangle$. Therefore, by choosing core orbital a as $3p_{3/2}$, $3p_{1/2}$, $3d_{3/2}$, and $3d_{5/2}$ from the configuration $[3p^6 3d^{10}]$, we can obtain the interested states of the Co-like ions using the above method. The amplitudes of the RCC operators R_a and energy of the resulting state are obtained using the following equations:

$$\langle \Phi_a^* | \widehat{H_N e^T} - \Delta E_a R_a | \Phi_a \rangle = -\langle \Phi_a^* | \widehat{H_N e^T} | \Phi_a \rangle, \quad (14)$$

and

$$\langle \Phi_a | \widehat{H_N e^T} \{1 + R_a\} | \Phi_a \rangle = \Delta E_a, \quad (15)$$

respectively, where $|\Phi_a^*\rangle$ corresponds to excited Slater determinants with respect to $|\Phi_a\rangle$ and $\Delta E_a = E_a - E_0$ [ionization potential (IP)] for the energy value E_a of the state $|\Psi_a\rangle$. It is evident from the above two equations that they are coupled to each other and, therefore, need to be solved simultaneously by adopting a self-consistent procedure. Also, by taking the differences between the ΔE_a values of different states, their excitation energies (EEs) can be evaluated. Furthermore, it is important to note that, due to the choice of the DHF wave function as the starting point, the initial solution (at the first iteration) of the above two equations will correspond to the results for the second-order RMBPT [RMBPT(2)] method.

In our calculations, we have considered only the dominant singles and doubles excitations in the RCC theory (RCCSD method) by defining $T = T_1 + T_2$ and $R_a = R_{1a} + R_{2a}$, where and subscripts 1 and 2 denote singles and doubles, respectively. To make use of the normal ordering and Wick's theorem to reduce the amount of computation, these RCC operators are defined using the second quantization operators as follows:

$$\begin{aligned} T_1 &= \sum_{a,p} a_p^\dagger a_a t_a^p, & T_2 &= \frac{1}{4} \sum_{ab,pq} a_p^\dagger a_q^\dagger a_b a_a t_{ab}^{pq}, \\ R_{1a} &= \sum_{b \neq a} a_b^\dagger a_a r_a^b, & R_{2a} &= \frac{1}{2} \sum_{bd,p} a_b^\dagger a_p^\dagger a_d a_a r_{ad}^{bp}, \end{aligned} \quad (16)$$

where the indices a, b and p, q represent for the core and virtual orbitals, respectively, the ts are the amplitudes for the T operators, and the rs are the amplitudes of the R_a operators.

Once atomic wave functions of the considered states of the Co-like ions are evaluated, transition matrix elements due to an operator O between the $|\Psi_f\rangle$ and $|\Psi_i\rangle$ states are determined by

$$\frac{\langle \Psi_f | O | \Psi_i \rangle}{\sqrt{\langle \Psi_f | \Psi_f \rangle \langle \Psi_i | \Psi_i \rangle}} = \frac{\langle \Phi_f | \{1 + R_f^\dagger\} \overline{O} \{1 + R_i\} | \Phi_i \rangle}{\sqrt{\mathcal{N}_f \mathcal{N}_i}}, \quad (17)$$

where $\bar{O} = (e^{T^\dagger} O e^T)_l$ and $\mathcal{N}_k = \{(1 + R_k^\dagger) \bar{\mathcal{N}} (1 + R_k)\}$, where the index $k = i$ and f , with $\bar{\mathcal{N}} = (e^{T^\dagger} e^T)_l$, for the subscript l meaning only the linked terms are contributing. It can be noted that the expectation value of the operator O can be estimated by considering both the initial and final wave functions as same in the above expression. In our earlier works (e.g., see Refs. [11,22,43]), we have discussed in detail the procedures to evaluate these terms. For better understanding of various contributions to the matrix elements, we explicitly quote the contributions from the normalizations of the wave functions using the following expression:

$$\begin{aligned} \text{norm} &= \left[\frac{\langle \Psi_f | O | \Psi_i \rangle}{\sqrt{\langle \Psi_f | \Psi_f \rangle \langle \Psi_i | \Psi_i \rangle}} - \langle \Psi_f | O | \Psi_i \rangle \right] \\ &= \left[\frac{1}{\sqrt{\mathcal{N}_f \mathcal{N}_i}} - 1 \right] \langle \Psi_f | O | \Psi_i \rangle. \end{aligned} \quad (18)$$

It is worth noting that calculations of $E1$ and $E2$ matrix elements using the length gauge expressions converge faster in an approximated many-body method over the velocity gauge expressions [44]. Therefore, we use the length gauge expressions [45] to evaluate the $E1$ and $E2$ matrix elements in the present work. Also, we use Gaussian-type orbitals (GTOs), as defined in Ref. [46], to obtain the single-particle orbitals. We have considered up to g -orbital angular-momentum symmetry (orbital angular momentum $l = 5$) to carry out all the calculations. We have used a sufficiently large number of GTOs such as $38s$, $37p$, $36d$, $35f$, and $34g$ for constructing the single-particle DHF orbitals. To perform the RCC calculations with the limited computational facility, we have, however, considered only $16s$, $15p$, $14d$, $13f$, and $12g$ active orbitals to account for the electron correlation effects.

IV. ATOMIC PROPERTIES OF INTEREST

A. Lifetime of atomic states

The spontaneous transition probabilities of a transition $|\Psi_i\rangle \rightarrow |\Psi_f\rangle$ due to the $E1$, electric-quadrupole ($E2$), and $M1$ channels are given by [39]

$$A_{i \rightarrow f}^{E1} = \frac{2.0261 \times 10^{-6}}{\lambda_{ik}^3 g_i} S_{if}^{E1}, \quad (19)$$

$$A_{i \rightarrow f}^{E2} = \frac{1.1195 \times 10^{-22}}{\lambda_{ik}^5 g_i} S_{if}^{E2}, \quad (20)$$

$$A_{i \rightarrow f}^{M1} = \frac{2.6971 \times 10^{-11}}{\lambda_{ik}^3 g_i} S_{if}^{M1}, \quad (21)$$

respectively, where the quantity $S_{if}^O = |\langle \Psi_f || O || \Psi_i \rangle|^2$ is the square of the reduced matrix element between the two states with O representing the corresponding $E1$, $E2$, or $M1$ transition operator. This is commonly known as the line strength of the electromagnetic transition and here we calculate them in a.u. The transition wavelength λ_{if} used in the above formulas are taken in centimeter and $g_i = 2J_i + 1$ is the degeneracy factor of the initial state $|\Psi_i\rangle$ with the angular momentum J_i . Thus, the transition probabilities determined using these formulas are finally given in s^{-1} .

Another, useful quantity which could be of particular interest in the astrophysical study is the emission (absorption)

oscillator strengths F_{if} (F_{fi}). This quantity can be deduced from the above transition probabilities through the following expressions [47]

$$F_{if}^O = 1.4992 \times 10^{-16} A_{if}^O \frac{g_i}{g_f} \lambda_{if}^2, \quad (22)$$

where λ_{if} and A_{if} are used in \AA and s^{-1} units, respectively. Also, the emission and absorption oscillator strengths satisfy the relation as $g_f F_{fi}^O = -g_i F_{if}^O$.

The lifetime of a given atomic state is the inverse of the total transition probabilities involving all possible spontaneous emission channels; i.e., the lifetime (in seconds corresponding to the units used above) of the state $|\Psi_f\rangle$ is given by

$$\tau_i = \frac{1}{\sum_{O,f} A_{i \rightarrow f}^O}, \quad (23)$$

where sum over O represents all possible decay channels due to transition operators O and the summation index f corresponds to all the final atomic states.

B. Hyperfine interaction coefficients

The Hamiltonian describing the noncentral form of hyperfine interaction between the electrons and nucleus in an atomic system is expressed in terms of spherical tensor operator products as [37,48]

$$H_{hf} = \sum_k \mathbf{M}_n^{(k)} \cdot \mathbf{O}_{hf}^{(k)}, \quad (24)$$

where $\mathbf{M}_n^{(k)}$ and $\mathbf{O}_{hf}^{(k)}$ are the spherical tensor operators with rank k (>0) in the nuclear and electronic coordinates, respectively. Since these interaction strengths become much weaker with higher values of k , we consider only up to $k = 2$ for the present interest. Also, we account only the first-order effects due to these interactions giving rise to the energy shift to an energy level

$$\begin{aligned} W_{F,J} = \langle H_{hf} \rangle &= A_{hf} \mathbf{I} \cdot \mathbf{J} \\ &+ B_{hf} \frac{3(\mathbf{I} \cdot \mathbf{J})^2 + \frac{3}{2}(\mathbf{I} \cdot \mathbf{J}) - I(I+1)J(J+1)}{2I(2I-1)J(2J-1)}, \end{aligned} \quad (25)$$

where I and J are the nuclear and atomic angular momenta, respectively, and A_{hf} and B_{hf} are known as the $M1$ and $E2$ hyperfine structure constants respectively. With the knowledge of A_{hf} and B_{hf} , it is possible to estimate $W_{F,J}$ for any hyperfine level $F = I + J$. Thus, we evaluate these constants using the expressions

$$A_{hf} = \mu_N g_I \frac{\langle J || O_{hf}^{(1)} || J \rangle}{\sqrt{J(J+1)(2J+1)}}, \quad (26)$$

and

$$\begin{aligned} B_{hf} &= 2Q_I \left[\frac{2J(2J-1)}{(2J+1)(2J+2)(2J+3)} \right]^{1/2} \\ &\times \langle J || O_{hf}^{(2)} || J \rangle, \end{aligned} \quad (27)$$

where μ_N is the nuclear Bohr magneton, $g_I = \frac{\mu_I}{I}$, μ_I and Q_I are the nuclear $M1$ and $E2$ moments, respectively. Since the A_{hf}/g_I and B_{hf}/Q_I values are independent of isotopes and

TABLE I. (upper panel) The ionization potential (IPs) (in cm^{-1}) for removing one electron from the $3d_{5/2}$ orbital of the Ni-like closed-shell configuration $3p^6 3d^{10}$ to construct the ground state $3p^6 3d^9 {}^2D_{5/2}$ for Co-like ions from Y-Cd. Contributions from the Breit, VP (Uehling + Wichmann Kroll) and SE (both from the electric and magnetic form factors) effects are given as ΔE_B , ΔE_{VP} , and ΔE_{SE} , respectively. The IPs obtained using the DC Hamiltonian are also given at different levels of approximations such as the DHF, RMBPT(2), and RCCSD methods. The final IP values are obtained by adding the RCCSD values from the DC Hamiltonian and other relativistic corrections, and finally compared with the NIST values [34]. (lower panel) Excitation energies (EEs) (in cm^{-1}) for the four low-lying atomic states $3p^6 3d^9 {}^2D_{5/2,3/2}$ and $3p^5 3d^{10} {}^2P_{1/2,3/2}$ in the Co-like ions Y^{12+} , Zr^{13+} , Nb^{14+} , Mo^{15+} , Tc^{16+} , Ru^{17+} , Rh^{18+} , Pd^{19+} , Ag^{20+} , and Cd^{21+} . Similar to the ground-state IP, for EE, contributions from Breit, VP, and SE interactions are also given explicitly as ΔE_B , ΔE_{VP} , and ΔE_{SE} , respectively. The EEs obtained using the DC Hamiltonian are also given at different levels of approximation such as the DHF, RMBPT(2) and RCCSD methods. The final EEs are given by combining the contributions from Breit and QED corrections to the RCCSD values obtained with the H_{DC} Hamiltonian. The values given under “fitted” are the extrapolated values reported in the literature by combining calculations using the MCDHF method and the observed wavelength values [29]. The results given as “Expt.” denote the experimental EEs obtained from direct measurements [27,28].

Ionization potentials (IPs)											
	IPs (with H_{DC})			ΔE_B	ΔE_{VP}	ΔE_{SE}	IP (final)	NIST			
	DHF	RMBPT	RCCSD								
Y^{12+}	3 035 558	3 006 606	3 015 229	-323	-13	131	3 015 024(2000)	3 016 800(2000)			
Zr^{13+}	3 465 335	3 436 867	3 444 895	-459	-15	104	3 444 525(1800)	3 436 000(21000)			
Nb^{14+}	3 920 121	3 892 095	3 899 604	-615	-16	162	3 899 135(1780)	3 892 000(12000)			
Mo^{15+}	4 399 869	4 372 259	4 379 311	-792	-19	187	4 378 686(1660)	4 388 000(4000)			
Tc^{16+}	4 904 541	4 877 323	4 883 968	-992	-21	237	4 883 191(1600)	4 872 000(21000)			
Ru^{17+}	5 434 085	5 407 228	5 413 510	-1214	-24	221	5 412 492(1570)	5 404 000(23000)			
Rh^{18+}	5 988 428	5 961 888	5 967 851	-1460	-27	232	5 966 596(1500)	5 960 000(24000)			
Pd^{19+}	6 567 479	6 541 206	6 546 886	-1730	-30	226	6 545 351(1580)	6 533 000(25000)			
Ag^{20+}	7 171 144	7 145 090	7 150 516	-2026	-33	-148	7 148 307(1500)	7 138 000(30000)			
Cd^{21+}	7 799 345	7 773 465	7 778 662	-2350	-36	304	7 776 580(1580)	7 767 000(30000)			
Excitation energies (EEs)											
State	EE (with H_{DC})			ΔE_B	ΔE_{VP}	ΔE_{SE}	EE (Final)	Expt.	Fitted ^a		
	DHF	RMBPT	RCCSD								
Y^{12+}											
$3p^6 3d^9 {}^2D_{5/2}$	0.0	0.0	0.0	0.0	0.0	0.0	0.0	0.0	0.0		
$3p^6 3d^9 {}^2D_{3/2}$	18526	17686	17896	-718	≈ 0.0	90	17 267(40)			17 240(10)	
$3p^5 3d^{10} {}^2P_{3/2}$	1 171 572	1 144 269	1 146 876	-2341	-4.0	-154	1 144 377(190)			1 144 220(70)	
$3p^5 3d^{10} {}^2P_{1/2}$	1 274 772	1 243 333	1 246 927	-4049	≈ 0.0	188	1 243 066(220)			1 242 580(80)	
Zr^{13+}											
$3p^6 3d^9 {}^2D_{5/2}$	0.0	0.0	0.0	0.0	0.0	0.0	0.0	0.0	0.0		
$3p^6 3d^9 {}^2D_{3/2}$	21 532	20 673	20 877	-808	≈ 0.0	156	20 224(45)	20 131(1.0) ^b		20 125(1.2)	
$3p^5 3d^{10} {}^2P_{3/2}$	1 228 597	1 202 599	1 204 773	-2577	-3.0	-235	1 201 956(210)			1 201 940(70)	
$3p^5 3d^{10} {}^2P_{1/2}$	1 346 218	1 316 170	1 319 203	-4485	-4.0	397	1 315 116(230)			1 314 590(80)	
Nb^{14+}											
$3p^6 3d^9 {}^2D_{5/2}$	0.0	0.0	0.0	0.0	0.0	0.0	0.0	0.0	0.0		
$3p^6 3d^9 {}^2D_{3/2}$	24 888	24 006	24 206	-906	-1.0	39	23 338(50)	23 369(5.0) ^c		23 363(5)	
$3p^5 3d^{10} {}^2P_{3/2}$	1 285 998	1 261 072	1 262 928	-2829	-4.0	-142	1 259 953(220)			1 259 890(80)	
$3p^5 3d^{10} {}^2P_{1/2}$	1 419 551	1 390 580	1 393 222	-4950	-1.0	-42	1 388 232(245)			1 388 250(90)	
Mo^{15+}											
$3p^6 3d^9 {}^2D_{5/2}$	0.0	0.0	0.0	0.0	0.0	0.0	0.0	0.0	0.0		
$3p^6 3d^9 {}^2D_{3/2}$	28 618	27 711	27 907	-1011	≈ 0.0	37	26 933(60)	26 967(2.0) ^b		26 960(1.5)	
$3p^5 3d^{10} {}^2P_{3/2}$	1 343 785	1 319 765	1 321 378	-3094	-4.0	-160	1 318 121(230)			1 318 110(90)	
$3p^5 3d^{10} {}^2P_{1/2}$	1 494 890	1 466 788	1 469 137	-5445	-3.0	-83	1 463 612(255)			1 463 760(100)	
Tc^{16+}											
$3p^6 3d^9 {}^2D_{5/2}$	0.0	0.0	0.0	0.0	0.0	0.0	0.0	0.0	0.0		
$3p^6 3d^9 {}^2D_{3/2}$	32 748	31 814	32 008	-1123	-1.0	11	30 896(50)			30 950(30)	
$3p^5 3d^{10} {}^2P_{3/2}$	1 401 982	1 378 742	1 380 163	-3373	-4.0	-158	1 376 628(240)			1 376 670(90)	
$3p^5 3d^{10} {}^2P_{1/2}$	1 572 370	1 544 984	1 547 106	-5972	-4.0	-218	1 540 920(260)			1 541 270(120)	

TABLE I. (Continued.)

State	EE (with H_{DC})			ΔE_B	ΔE_{VP}	ΔE_{SE}	EE (Final)	Expt.	Fitted ^a
	DHF	RMBPT	RCCSD						
Ru ¹⁷⁺									
$3p^6 3d^9 2D_{5/2}$	0.0	0.0	0.0	0.0	-0.0	0.0	0.0	0.0	0.0
$3p^6 3d^9 2D_{3/2}$	37 305	36 341	36 535	-1244	-1.0	131	35 421(60)		35 360(40)
$3p^5 3d^{10} 2P_{3/2}$	1 460 623	1 438 060	1 439 327	-3668	-4.0	-286	1 435 367(250)		1 435 610(100)
$3p^5 3d^{10} 2P_{1/2}$	1 652 147	1 625 353	1 627 294	-6533	-5.0	-586	1 620 911(270)		1 621 000(130)
Rh ¹⁸⁺									
$3p^6 3d^9 2D_{5/2}$	0.0	0.0	0.0	0.0	0.0	0.0	0.0	0.0	0.0
$3p^6 3d^9 2D_{3/2}$	42 319	41 324	41 515	-1373	-1.0	163	40 304(70)		40 230(40)
$3p^5 3d^{10} 2P_{3/2}$	1 519 753	1 497 785	1 498 922	-3979	-5.0	-340	1 494 597(255)		1 494 970(110)
$3p^5 3d^{10} 2P_{1/2}$	1 734 390	1 708 088	1 709 879	-7129	8.0	200	1 702 961(275)		1 703 130(140)
Pd ¹⁹⁺									
$3p^6 3d^9 2D_{5/2}$	0.0	0.0	0.0	0.0	0.0	0.0	0.0	0.0	0.0
$3p^6 3d^9 2D_{3/2}$	47 819	46 791	46 980	-1511	-1.0	218	45 686(70)		45 580(50)
$3p^5 3d^{10} 2P_{3/2}$	1 579 427	1 557 983	1 559 011	-4306	-4.0	-417	1 554 283(260)		1 554 850(120)
$3p^5 3d^{10} 2P_{1/2}$	1 819 281	1 793 387	1 795 053	-7761	10.0	339	1 787 641(280)		1 787 800(160)
Ag ²⁰⁺									
$3p^6 3d^9 2D_{5/2}$	0.0	0.0	0.0	0.0	0.0	0.0	0.0	0.0	0.0
$3p^6 3d^9 2D_{3/2}$	53 837	52 771	52 961	-1658	≈0.0	539	51 842(72)		51 430(50)
$3p^5 3d^{10} 2P_{3/2}$	1 639 699	1 618 718	1 619 653	-4650	-7.0	-723	1 614 278(275)		1 615 220(130)
$3p^5 3d^{10} 2P_{1/2}$	1 907 009	1 881 449	1 883 010	-8431	12.0	1561	1 876 154(285)		1 875 220(170)
Cd ²¹⁺									
$3p^6 3d^9 2D_{5/2}$	0.0	0.0	0.0	0.0	0.0	0.0	0.0	0.0	0.0
$3p^6 3d^9 2D_{3/2}$	60 402	59 299	59 489	-1814	-1.0	133	57 807(80)		57 810(60)
$3p^5 3d^{10} 2P_{3/2}$	1 700 622	1 680 052	1 680 910	-5009	-4.0	-413	1 675 481(280)		1 676 160(140)
$3p^5 3d^{10} 2P_{1/2}$	1 997 763	1 972 475	1 973 948	-9139	15.0	-73	1 964 751(290)		1 965 520(190)

^aReference [29].^bReference [26].^cReference [27].

depend only on the atomic wave functions, determination of these quantities are our particular interest.

V. RESULTS AND DISCUSSION

We first discuss the IP for the $5d_{5/2}$ orbital in the closed-shell configuration of the Ni isoelectronic sequence which eventually leads to the ground state for the Co-like ions. In this process, we obtain the first IPs of the respective Ni-like ions. These IPs are given in the upper panel of Table I. To see the flow of electron correlation effect, we calculate the ground state IP at different levels of approximation namely DHF, RMBPT, and RCCSD using the H_{DC} Hamiltonian. In the next approximation, we include the effect from Breit, VP and SE interaction on top of the H_{DC} Hamiltonian. These contributions are given distinctly as Breit interaction (ΔE_B), VP effect (ΔE_{VP}), and SE effect (ΔE_{SE}). Our final IP value [denoted “IP (Final)” in Table I] for the ground state are thus determined using the H_{DCBVS} approximation. We also estimate uncertainties to the final RCCSD IP values by analyzing contributions due to the truncation of basis functions and neglected higher-level excitations in the RCC theory. The basis function extrapolations are obtained using a lower-order many-body method while we have estimated uncertainties due to the higher level excitations by analyzing contributions from the dominant

triple excitations by adopting the perturbative approach. Our final values are also compared with the IPs of the only available data for the $3p^6 3d^9 2D_{5/2}$ states for all the ions from the National Institute of Science and Technology (NIST) database [34]. The NIST values were obtained using the nonrelativistic Hartree-Fock orbitals, so we see large differences among these values. IPs for the orbitals giving rise to the other states of Co-like ions are not available for comparison.

Similarly, the IPs for the orbitals $d_{3/2}$, $p_{3/2}$, and $p_{1/2}$ give rise to the other three excited states such as $3p^6 3d^9 2D_{5/2}$, $3p^6 3d^9 2D_{3/2}$, $3p^5 3d^{10} 2P_{3/2}$, and $3p^5 3d^{10} 2P_{1/2}$ of the investigated Co-like ions. However, in the experiment, the more relevant quantities are the EEs which are defined with respect to the ground-state IP value. In this context, we directly give the EEs for the considered three excited states by taking the difference in the respective IP values from the ground-state IP. In the lower panel of Table I, we present the comprehensive information on these EEs. We first extract the EEs from IPs that are systematically calculated using DHF, RMBPT, and RCCSD methods at the DC approximation. Contributions from the leading-order relativistic corrections such as ΔE_B , ΔE_{VP} , and ΔE_{SE} are also estimated and quoted in the above table explicitly. From these tabulated values for EEs, we find after the Coulomb interactions the Breit interactions also contribute significantly to the energy. There are large

TABLE II. Transition properties such as wavelengths λ (in nm), line strengths S_{if}^O (in a.u.), weighted oscillator strengths $g_f F_{if}^O$, and transition rates A_{if}^O (in s^{-1}) due to different channels (O) for the five low-lying transitions among the atomic states calculated in this work. The values obtained using our RCCSD method are denoted ‘‘This work’’ and are compared with the previously reported values using the MCDHF method [32]. The column denoted ‘‘Expt.’’ represents the experimental wavelengths taken from Refs. [26,27,42] for Y^{12+} – Mo^{15+} ions and for Ru^{17+} – Cd^{21+} ions from Ref. [29].

Transition (O)	λ (nm)		S_{if}^O		$g_f F_{if}^O$		A_{if}^O	
	This work	Expt.	This work	Ref. [32]	This work	Ref. [32]	This work	Ref. [32]
Y^{12+}								
$^2D_{3/2} \xrightarrow{M1} ^2D_{5/2}$	579.11(5)		2.541(20)	2.395	1.771(22)[–6]	1.670[–6]	87.802(40)	82.72
$\xrightarrow{E2} ^2D_{5/2}$			0.0198(10)		1.705(10)[–11]		8.4521(20)[–4]	
$^2P_{3/2} \xrightarrow{E1} ^2D_{3/2}$	8.8721(6)	8.8731(5) ^a	0.0387(12)		0.156(7)		2.8102(6)[10]	
$\xrightarrow{E1} ^2D_{5/2}$	8.7383(5)	8.7394(5) ^a	0.352(13)		1.218(10)		2.6781(7)[11]	
$^2P_{1/2} \xrightarrow{M1} ^2P_{3/2}$	101.320(10)		1.490(15)		5.928(25)[–6]		1.9121(20)[4]	
$\xrightarrow{E2} ^2P_{3/2}$			0.0429(8)		8.056(30)[–9]		26.0002(25)	
$\xrightarrow{E1} ^2D_{3/2}$	8.1582(7)	8.1610(5) ^a	0.191(7)		0.708(12)		3.5710(7)[11]	
Zr^{13+}								
$^2D_{3/2} \xrightarrow{M1} ^2D_{5/2}$	494.42(10)	496.74(3) ^b	2.529(22)	2.395	2.058(20)[–6]	1.670[–6]	139.12(25)	131.6
$\xrightarrow{E2} ^2D_{5/2}$			0.0163(7)		2.239(25)[–11]		0.0015(3)	
$^2P_{3/2} \xrightarrow{E1} ^2D_{3/2}$	8.4622(8)	8.4612(5) ^a	0.0357(9)		0.1268(15)		2.9861(5)[10]	
$\xrightarrow{E1} ^2D_{5/2}$	8.3203(7)	8.3196(5) ^a	0.325(10)		1.188(12)		2.8622(6)[11]	
$^2P_{1/2} \xrightarrow{M1} ^2P_{3/2}$	88.3701(12)		1.466(13)		6.680(20)[–6]		2.8281(12)[4]	
$\xrightarrow{E2} ^2P_{3/2}$			0.0429(8)		1.029(7)[–8]		43.5690(15)	
$\xrightarrow{E1} ^2D_{3/2}$	7.7226(10)	7.7249(5) ^a	0.176(7)		0.688(11)		3.8681(7)[11]	
Nb^{14+}								
$^2D_{3/2} \xrightarrow{M1} ^2D_{5/2}$	428.49(12)	427.91(9) ^c	2.518(22)	2.395	2.379(24)[–6]	2.263[–6]	216.71(22)	205.7
$\xrightarrow{E2} ^2D_{5/2}$			0.0136(8)		2.920(26)[–11]		0.0266(7)	
$^2P_{3/2} \xrightarrow{E1} ^2D_{3/2}$	8.0865(6)	8.0871(5) ^a	0.0331(6)		0.124(5)		3.1681(6)[10]	
$\xrightarrow{E1} ^2D_{5/2}$	7.9368(7)	7.9374(5) ^a	0.301(7)		1.152(10)		3.0520(7)[11]	
$^2P_{1/2} \xrightarrow{M1} ^2P_{3/2}$	77.955(13)		1.449(13)		7.520(20)[–6]		4.1333(13)[4]	
$\xrightarrow{E2} ^2P_{3/2}$			0.0368(8)		1.305(13)[–8]		71.7453(10)	
$\xrightarrow{E1} ^2D_{3/2}$	7.3262(7)	7.3273(5) ^a	0.162(7)		0.668(10)		4.1902(7)[11]	
Mo^{15+}								
$^2D_{3/2} \xrightarrow{M1} ^2D_{5/2}$	371.30(13)	370.81(02) ^b	2.508(18)	2.394	2.735(25)[–6]	2.610[–6]	331.74(30)	316.3
$\xrightarrow{E2} ^2D_{5/2}$			0.0115(3)		3.774(30)[–11]		0.0046(6)	
$^2P_{3/2} \xrightarrow{E1} ^2D_{3/2}$	7.7453(7)	7.7456(5) ^a	0.0307(5)		0.128(7)		3.3492(5)[10]	
$\xrightarrow{E1} ^2D_{5/2}$	7.5862(7)	7.5869(5) ^a	0.279(6)		1.104(8)		3.2471(6)[11]	
$^2P_{1/2} \xrightarrow{M1} ^2P_{3/2}$	68.733(10)		1.435(11)		8.452(20)[–6]		5.9802(14)[4]	
$\xrightarrow{E2} ^2P_{3/2}$			0.0317(5)		1.645(26)[–8]		116.4311(12)	
$\xrightarrow{E1} ^2D_{3/2}$	6.9604(5)	6.9596(5) ^a	0.150(4)		0.656(6)		4.5362(7)[11]	
Tc^{16+}								
$^2D_{3/2} \xrightarrow{M1} ^2D_{5/2}$	323.66(9)		2.500(17)	2.394	3.128(22)[–6]	2.996[–6]	500.00(60)	478.5
$\xrightarrow{E2} ^2D_{5/2}$			0.010(4)		4.837(30)[–11]		0.0077(8)	
$^2P_{3/2} \xrightarrow{E1} ^2D_{3/2}$	7.4313(6)		0.0286(5)		0.120(4)		3.5330(6)[10]	
$\xrightarrow{E1} ^2D_{5/2}$	7.2642(7)		0.261(8)		1.086(7)		3.4482(6)[11]	
$^2P_{1/2} \xrightarrow{M1} ^2P_{3/2}$	60.867(11)		1.424(10)		9.476(15)[–6]		8.5621(16)[4]	
$\xrightarrow{E2} ^2P_{3/2}$			0.0275(5)		2.050(20)[–8]		185.2142(15)	
$\xrightarrow{E1} ^2D_{3/2}$	6.6224(8)		0.140(6)		0.640(6)		4.9073(7)[11]	
Ru^{17+}								
$^2D_{3/2} \xrightarrow{M1} ^2D_{5/2}$	282.32(8)		2.492(18)	2.393	3.562(15)[–6]	3.422[–6]	742.92(45)	713.6
$\xrightarrow{E2} ^2D_{5/2}$			0.0083(4)		1.162(25)[–11]		0.0132(8)	

TABLE II. (Continued.)

Transition (O)	λ (nm)		S_{if}^O		$g_f F_{if}^O$		A_{if}^O	
	This work	Expt.	This work	Ref. [32]	This work	Ref. [32]	This work	Ref. [32]
${}^2P_{3/2} \xrightarrow{E1} {}^2D_{3/2}$	7.1432(7)	7.1409(10) ^d	0.0267(8)		0.1124(8)		3.7173(5)[10]	
$\xrightarrow{E1} {}^2D_{5/2}$	6.9671(8)	6.9656(10) ^d	0.244(10)		1.062(7)		3.6544(5)[11]	
${}^2P_{1/2} \xrightarrow{M1} {}^2P_{3/2}$	53.895(10)		1.414(12)		1.060(6)[-5]		1.2152(12)[5]	
$\xrightarrow{E2} {}^2P_{3/2}$			0.0240(5)		2.569(20)[-8]		294.502(15)	
$\xrightarrow{E1} {}^2D_{3/2}$	6.3071(9)	6.3063(10) ^d	0.131(4)		0.628(7)		5.3035(6)[11]	
Rh¹⁸⁺								
${}^2D_{3/2} \xrightarrow{M1} {}^2D_{5/2}$	248.11(7)		2.485(22)	2.393	4.042(20)[-6]	3.892[-6]	1091(3)	1050
$\xrightarrow{E2} {}^2D_{5/2}$			0.0071(5)		7.800(25)[-11]		0.0210(5)	
${}^2P_{3/2} \xrightarrow{E1} {}^2D_{3/2}$	6.8762(9)	6.8739(10) ^d	0.0250(6)		0.1104(7)		3.9033(6)[10]	
$\xrightarrow{E1} {}^2D_{5/2}$	6.6912(8)	6.6889(10) ^d	0.228(6)		1.038(6)		3.8665(7)[11]	
${}^2P_{1/2} \xrightarrow{M1} {}^2P_{3/2}$	47.993(13)		1.405(10)		1.183(4)[-5]		1.7107(12)[5]	
$\xrightarrow{E2} {}^2P_{3/2}$			0.0210(7)		3.188(6)[-8]		460.783(16)	
$\xrightarrow{E1} {}^2D_{3/2}$	6.0144(11)	6.0133(10) ^d	0.123(5)		0.616(8)		5.7274(6)[11]	
Pd¹⁹⁺								
${}^2D_{3/2} \xrightarrow{M1} {}^2D_{5/2}$	218.90(15)		2.478(22)	2.392	4.567(20)[-6]	4.408(30)[-6]	1582.40	1526
$\xrightarrow{E2} {}^2D_{5/2}$			0.0062(3)		9.822(30)[-11]		0.0340(7)	
${}^2P_{3/2} \xrightarrow{E1} {}^2D_{3/2}$	6.6293(16)	6.6259(10) ^d	0.0235(4)		0.1068(7)		4.0883(6)[10]	
$\xrightarrow{E1} {}^2D_{5/2}$	6.4342(14)	6.4318(10) ^d	0.215(6)		1.002(5)		4.0854(7)[11]	
${}^2P_{1/2} \xrightarrow{M1} {}^2P_{3/2}$	42.853(12)		1.398(12)		6.312(10)[-6]		2.6243(15)[5]	
$\xrightarrow{E2} {}^2P_{3/2}$			0.0185(6)		3.955(20)[-8]		718.453(13)	
$\xrightarrow{E1} {}^2D_{3/2}$	5.7414(9)	5.7396(10) ^d	0.115(7)		0.608(8)		6.1825(6)[11]	
Ag²⁰⁺								
${}^2D_{3/2} \xrightarrow{M1} {}^2D_{5/2}$	192.90(12)		2.472(13)	2.392	5.141(20)[-6]	4.972(30)[-6]	2267.84	2191
$\xrightarrow{E2} {}^2D_{5/2}$			0.0053(4)		1.228(26)[-10]		0.0542(10)	
${}^2P_{3/2} \xrightarrow{E1} {}^2D_{3/2}$	6.4003(15)	6.3946(10) ^d	0.0221(5)		0.104(3)		4.2753(5)[10]	
$\xrightarrow{E1} {}^2D_{5/2}$	6.1952(13)	6.1913(10) ^d	0.202(7)		1.000(6)		4.3095(7)[11]	
${}^2P_{1/2} \xrightarrow{M1} {}^2P_{3/2}$	38.186(14)		1.392(11)		1.463(6)[-5]		3.3003(12)[5]	
$\xrightarrow{E2} {}^2P_{3/2}$			0.0164(5)		4.836(8)[-8]		1090.482(15)	
$\xrightarrow{E1} {}^2D_{3/2}$	5.4813(12)	5.4832(10) ^d	0.108(4)		0.596(7)		6.6716(6)[11]	
Cd²¹⁺								
${}^2D_{3/2} \xrightarrow{M1} {}^2D_{5/2}$	173.10(9)		2.467(20)	2.391	5.767(22)[-6]	5.588(60)[-6]	3213.74	3111
$\xrightarrow{E2} {}^2D_{5/2}$			0.0047(5)		1.527(30)[-10]		0.0851(8)	
${}^2P_{3/2} \xrightarrow{E1} {}^2D_{3/2}$	6.1824(12)	6.1789(10) ^d	0.0208(5)		0.104(4)		4.4733(6)[10]	
$\xrightarrow{E1} {}^2D_{5/2}$	5.9682(9)	5.9659(10) ^d	0.191(8)		0.972(8)		4.5457(7)[11]	
${}^2P_{1/2} \xrightarrow{M1} {}^2P_{3/2}$	34.570(13)		1.386(14)		1.622(10)[-5]		4.5294(15)[5]	
$\xrightarrow{E2} {}^2P_{3/2}$			0.0145(4)		5.916(18)[-8]		1652.603(15)	
$\xrightarrow{E1} {}^2D_{3/2}$	5.2439(11)	5.2416(10) ^d	0.102(6)		0.588(7)		7.1966(7)[11]	

^aReference [42].^bReference [26].^cReference [27].^dReference [29].

cancellations among the VP and SE effects of the QED interactions. These EE values also show that the DHF method overestimates the energies, while the corresponding values are significantly smaller for the RMBPT(2) and RCCSD methods using the DC Hamiltonian. Further analysis demonstrates contributions from the correlation and the relativistic effects

are increasing from the first-excited state to the third-excited state. The trends of the correlation effects are found to be similar in all the considered Co-like ions using our RCC theory. The values given inside the parentheses represent the maximum uncertainties associated with these EE results are calculated by adopting the same procedure as for the ground

TABLE III. The estimated lifetimes τ_i (in seconds) for the excited atomic states $3p^63d^9\ ^2D_{3/2}$, $3p^53d^{10}\ ^2P_{3/2}$, and $3p^53d^{10}\ ^2P_{1/2}$ using the total transition probabilities listed in Table II. Our result for the first-excited state is also compared with the other theoretical calculation by Ref. [32] for all the ions.

	$3p^63d^9\ ^2D_{3/2}$		$3p^53d^{10}\ ^2P_{3/2}$	$3p^53d^{10}\ ^2P_{1/2}$
	This work	Ref. [32]	This work	This work
Y ¹²⁺	1.139(10)[-2]	1.21[-2]	3.380(20)[-12]	2.800(30)[-12]
Zr ¹³⁺	7.187(12)[-3]	7.60[-3]	3.164(25)[-12]	2.585(30)[-12]
Nb ¹⁴⁺	4.614(14)[-3]	4.86[-3]	2.971(30)[-12]	2.386(40)[-12]
Mo ¹⁵⁺	3.014(14)[-3]	3.16[-3]	2.793(35)[-12]	2.204(40)[-12]
Tc ¹⁶⁺	2.001(12)[-3]	2.09[-3]	2.631(40)[-12]	2.038(50)[-12]
Ru ¹⁷⁺	1.346(11)[-3]	1.40[-3]	2.484(50)[-12]	1.886(60)[-12]
Rh ¹⁸⁺	9.166(20)[-4]	9.53[-4]	2.349(65)[-12]	1.746(65)[-12]
Pd ¹⁹⁺	6.319(15)[-4]	6.55[-4]	2.224(60)[-12]	1.617(60)[-12]
Ag ²⁰⁺	4.409(25)[-4]	4.56[-4]	2.112(60)[-12]	1.500(55)[-12]
Cd ²¹⁺	3.111(14)[-4]	3.21[-4]	2.002(55)[-12]	1.390(70)[-12]

IP values. In Table I, we also compare our calculated EEs with a few available experimental results. Only a few direct measurements of excitation energies are reported, while the other experimental values are extrapolated by fitting the calculated wavelengths with some of the observed wavelengths. So far, the direct measurements were carried out only for the ions Zr¹³⁺, Mo¹⁵⁺, and Nb¹⁴⁺. Edlén [28] had measured the forbidden lines of the Zr¹³⁺ and Mo¹⁵⁺ ions in a hot tokamak plasma experiment, while Prior [27] had directly obtained the EEs of Nb¹⁴⁺ by performing measurement using the electron cyclotron resonance ion source. The indirectly inferred values are quoted in the above table as “fitted,” which had used calculations using the MCDHF method to extrapolate EEs of all the considered ions [29]. Comparison between our calculated values with the measurements shows good agreement between them, suggesting our calculations for the transition matrix elements using the RCC theory can be accurate enough to estimate the transition properties of the excited states. This also suggests that the inclusion of triple excitations in our RCC calculations can improve our results further.

After analyzing the accuracies of the calculated EEs using our RCCSD method, we now proceed to calculate other transition properties such as the line strengths, transition probabilities, oscillator strengths, and lifetimes of the excited states of the considered Co-like ions. We also present the hyperfine structure constants of all the calculated states. The transition properties such as the line strengths, oscillator strengths, and transition probabilities are reported in the Table II and lifetimes of the excited states are presented in Table III. The line strengths are determined using the calculated reduced matrix elements of the $E1$, $E2$, and $M1$ operators in the length gauge. Combining the line strength results with the wavelengths we obtained the other transition properties.

In Table II, we also compare our calculated wavelengths with the available measured values. In Mo¹⁵⁺, our calculated wavelengths for the forbidden $M1$ transition within the ground-state doublet are in good agreement with the experimentally identified wavelengths by Suckewer *et al.*

in the Princeton Large Torus tokamak plasma [26]. For the same transition in Zr¹³⁺, we found that our estimated value of 494.42 nm is slightly smaller than the observed value of 496.74(3) nm [26]. Similarly, our calculated wavelength for this $M1$ transition in Nb¹⁴⁺ is in good agreement with its measured value using the electron cyclotron resonance ion source experiment by Prior *et al.* [27]. On the theoretical side, our results for the ground-state $M1$ line wavelengths are quite comparable with the MCDHF results reported by Guo *et al.* [32] for all the considered ions. There are also a few other calculations available for the Zr¹³⁺, Nb¹⁴⁺, and Mo¹⁵⁺ ions using different methods such as RMBPT and MCDHF [32] that show larger values of wavelengths from the experimental ones in this forbidden transition. Comparing our calculated wavelengths for the other four transitions considered, such as $3p^53d^{10}\ ^2P_{3/2} \rightarrow 3p^63d^9\ ^2D_{3/2}$, $3p^53d^{10}\ ^2P_{3/2} \rightarrow 3p^63d^9\ ^2D_{5/2}$, $3p^53d^{10}\ ^2P_{1/2} \rightarrow 3p^63d^9\ ^2D_{3/2}$, and $3p^53d^{10}\ ^2P_{1/2} \rightarrow 3p^53d^{10}\ ^2P_{3/2}$ with the available experimental values also shows excellent agreement between each other. For instance, Ryabtsev *et al.* observed wavelengths for the Y¹²⁺, Zr¹³⁺, Nb¹⁴⁺, and Mo¹⁵⁺ ions for these transitions using their low-inductance vacuum spark experiment [42]. Similarly, Ekberg *et al.* observed these first three transitions in Ru¹⁷⁺, Rh¹⁸⁺, Pd¹⁹⁺, Ag²⁰⁺, and Cd²¹⁺ ions using their laser-produced plasma experiment [29].

To reduce the uncertainties in other transition properties, we have used experimental wavelengths wherever available in estimating these quantities. Earlier, lifetimes of the fine-structure level of the ground state of the aforementioned ions were estimated by applying the MCDHF method, and we found reasonable agreement among our values with the previously estimated values. In the earlier estimations, contributions from the $E2$ channel were neglected and our analysis shows that they are indeed small. The lifetimes of the $3p^53d^{10}\ ^2P_{3/2}$ and $3p^53d^{10}\ ^2P_{1/2}$ states are not available to date, so we are unable to make a comparative analysis of these values. In the determination of lifetimes of the $3p^53d^{10}\ ^2P_{1/2}$ states, we have also accounted for the transition probabilities due to the forbidden channels but their contributions are found to be negligibly small compared with the $E1$ probability contributions. The $E1$ transition probabilities of the $3p^53d^{10}\ ^2P_{3/2} \rightarrow 3p^63d^9\ ^2D_{5/2}$ transitions are found to be dominant over the $3p^53d^{10}\ ^2P_{1/2} \rightarrow 3p^63d^9\ ^2D_{5/2}$ transitions. Although there are two more $E1$ transitions allowed from the $3p^53d^{10}\ ^2P_{3/2}$ state than from $3p^53d^{10}\ ^2P_{1/2}$, the lifetimes of the $3p^53d^{10}\ ^2P_{1/2}$ states in the Co-like ions are found to be smaller than those of the $3p^53d^{10}\ ^2P_{3/2}$ states. We also find that the $E1$ transition probabilities are larger when the angular-momentum difference is $|\Delta J = 1|$ than $|\Delta J = 0|$. Furthermore, due to the monotonic increase in the energy gap between the $3p^53d^{10}\ ^2P_{3/2}$ and the $3p^63d^9\ ^2D_{5/2}$ ground state with the size of the ion, the transition probabilities gradually increase from Y¹²⁺ to Tc¹⁶⁺. This results in smaller values of the lifetimes of the atomic states with increasing ionic charge of the Co-like systems.

Now we turn to present the results for the hyperfine structure constants of the considered Co-like ions. The accuracies of the transition matrix elements discussed earlier depend on the accurate determinations of the wave functions in the asymptotic region while accuracies in the evaluation of the hy-

TABLE IV. The calculated ratios A_{hf}/g_I (in MHz) and B_{hf}/Q_I (in MHz/b) of the atomic $3p^63d^9\ ^2D_{5/2}$, $3p^63d^9\ ^2D_{3/2}$, $3p^53d^{10}\ ^2P_{3/2}$, and $3p^53d^{10}\ ^2P_{1/2}$ states of the Y^{12+} , Zr^{13+} , Nb^{14+} , Mo^{15+} , Tc^{16+} , Ru^{17+} , Rh^{18+} , Pd^{19+} , Ag^{20+} , and Cd^{21+} ions using the DHF and RCCSD methods. The B_{hf}/Q_I of the Y^{12+} , Ag^{20+} , and Cd^{21+} ions is not given because B_{hf} of these states is zero owing to their nuclear spin $I = 1/2$.

Ion	$\frac{A_{hf}}{g_I}$								$\frac{B_{hf}}{Q_I}$					
	$3p^63d^9\ ^2D_{5/2}$		$3p^63d^9\ ^2D_{3/2}$		$3p^53d^{10}\ ^2P_{3/2}$		$3p^53d^{10}\ ^2P_{1/2}$		$3p^63d^9\ ^2D_{5/2}$		$3p^63d^9\ ^2D_{3/2}$		$3p^53d^{10}\ ^2P_{3/2}$	
	DHF	RCCSD	DHF	RCCSD	DHF	RCCSD	DHF	RCCSD	DHF	RCCSD	DHF	RCCSD	DHF	RCCSD
Y^{12+}	2651	2753	6331	6904	14 925	16 355	86 147	93 936						
Zr^{13+}	2991	3102	7151	7765	16 587	18 077	96 486	104 668	6160	6242	4492	4555	31 357	33 487
Nb^{14+}	3361	3477	8036	8693	18 375	19 932	107 642	116 271	6919	7000	5056	5118	34 786	37 007
Mo^{15+}	3752	3881	8992	9691	20 291	21 921	119 794	128 922	7735	7813	5665	5726	38 461	40 782
Tc^{16+}	4176	4313	10 021	10 762	22 336	24 044	132 940	142 607	8611	8686	6321	6380	42 400	44 825
Ru^{17+}	4631	4775	11 121	11 911	24 517	26 308	147 227	157 478	9548	9618	7026	7082	46 604	49 141
Rh^{18+}	5113	5267	12 295	13 133	26 842	28 721	162 616	173 490						
Pd^{19+}	5627	5791	13 551	14 441	29 314	31 285	179 231	190 771	11 614	11 672	8591	8638	55 887	58 660
Ag^{20+}	6174	6346	14 891	15 831	31 935	34 004	197 381	209 651						
Cd^{21+}	6756	6941	16 312	17 304	34 724	36 892	216 274	229 276						

perfine structure constants depend on the accurate calculations of the wave functions in the nuclear region. The determination of the hyperfine structure constants not only depends on the accurate calculations of the atomic matrix elements but also requires knowledge of accurate values of the nuclear moments. Since we are interested to estimate the A_{hf} and B_{hf} values, we need prior knowledge of $g_I = \frac{\mu_I}{I}$ and Q_I of the isotopes of the interest. This implies the A_{hf} and B_{hf} values are isotope dependent. However, the calculations of the A_{hf}/g_I and B_{hf}/Q_I values hardly change with the nuclear structure of the isotopes of an element. Thus, we discuss first these results and then present the estimated A_{hf} and B_{hf} value only for the stable isotopes of the elements of the investigated Co-like ions by combining with their respective g_I and Q_I values. Our calculated values of A_{hf}/g_I and B_{hf}/Q_I are reported in Table IV for all the considered atomic states of the Co-like Y^{12+} - Cd^{21+} ions. We have not given the B_{hf}/Q_I values of the Y^{12+} , Rh^{18+} , Ag^{20+} , and Cd^{21+} ions because their B_{hf} values do not exist owing to the fact that they all have $I = 1/2$. It can be observed from this table that the DHF

values for A_{hf}/g_I are smaller than the RCCSD results for all the states, which are the opposite of the trends seen in the calculations of EEs. The values and the electron correlation effects increase from the ground to the higher excited states. The reason for the large magnitude is due to the fact that the $3d$ orbitals have less overlap with the nucleus than do the $3p$ orbitals, which are the valence orbitals of the first and the last two states, respectively. The possible reason for which the correlation effects are seen to be enhanced in the calculations of the hyperfine structure constants for the ground state to the higher level excited states are probably due to the large correlations among the s and p orbitals than the s and d orbitals. Again, the values of the above quantities are found to be increasing with the size of the ion. The reason for this could be due to highly contracted orbitals in the more highly charged ions that can overlap with the nucleus strongly.

We also intend to fathom the roles of different electron correlation effects in the atomic states of Co-like ions. Evaluation of transition matrix elements depends on the wave functions

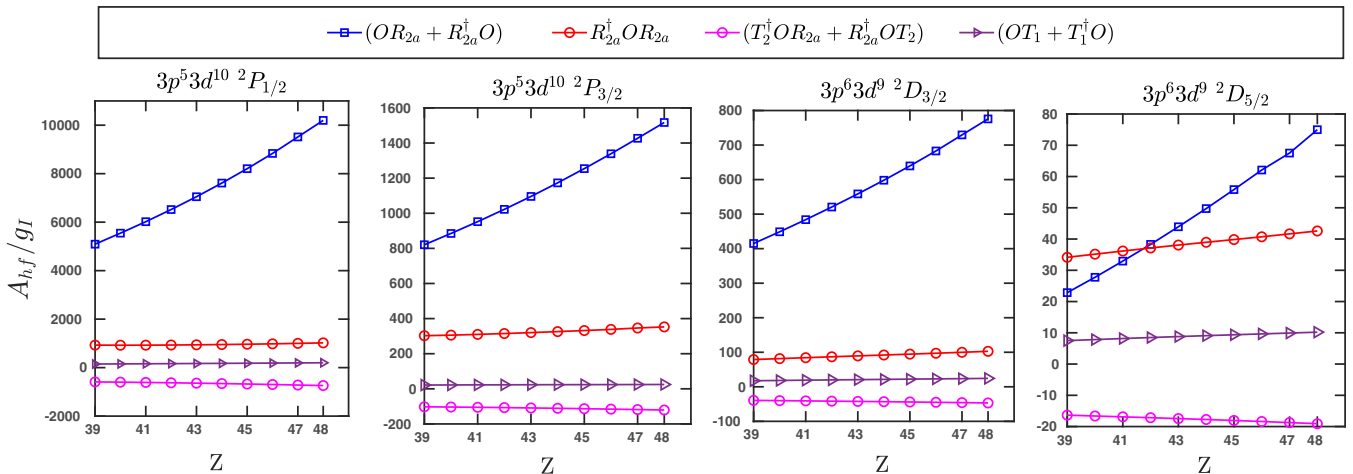


FIG. 1. Plots showing the contributions from different dominant RCC terms such as $(OR_{2a} + R_{2a}^\dagger O)$, $(OT_1 + T_1^\dagger O)$, $R_{2a}^\dagger OR_{2a}$, and $(R_{2a}^\dagger OT_2 + T_2^\dagger OR_{2a})$ in the calculations of the ratios A_{hf}/g_I (in MHz) for the calculated states against the atomic number Z of the considered ions.

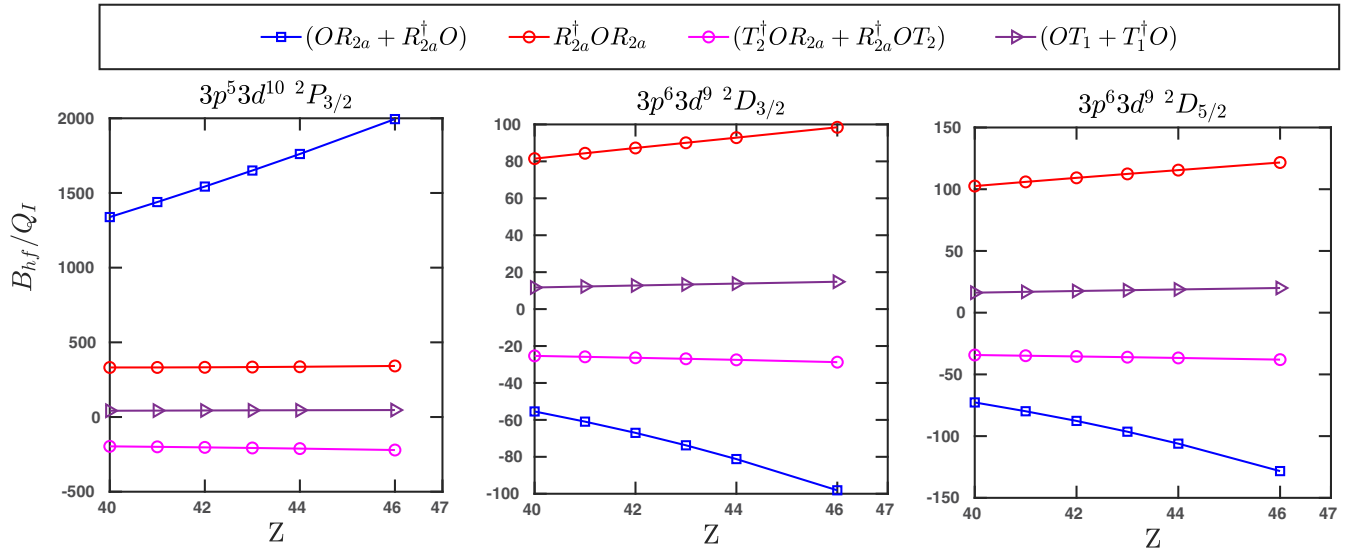


FIG. 2. Plots showing the contributions from different dominant RCC terms such as $(OR_{2a} + R_{2a}^\dagger O)$, $(OT_1 + T_1^\dagger O)$, $R_{2a}^\dagger OR_{2a}$, and $(R_{2a}^\dagger OT_2 + T_2^\dagger OR_{2a})$ in the evaluation of the ratios B_{hf}/Q_I (in MHz) against the atomic number Z of the Zr^{13+} , Nb^{14+} , Mo^{15+} , Tc^{16+} , Ru^{17+} , and Pd^{19+} ions. Since $I = 1/2$ for the ions $^{89}Y^{12+}$, $^{103}Rh^{18+}$, $^{109}Ag^{20+}$, and $^{111}Cd^{21+}$, the Q_I values for them do not exist. This is why we have excluded the calculation of the B_{hf}/Q_I ratios for these ions.

of two different atomic states, while the determination of hyperfine structure constants of a state depends only on the wave function of the respective state. Thus, we analyze the contributions to the A_{hf}/g_I and B_{hf}/Q_I values arising through various RCCSD terms. Instead of quoting them in tables, we show their contributions to the A_{hf}/g_I and B_{hf}/Q_I values in the graphical representations in Figs. 1 and 2, respectively, against the atomic number. Among all property-evaluating RCC terms, we find that the OR_{2a} , OT_1 , $R_{2a}^\dagger OR_{2a}$, and $R_{2a}^\dagger OT_2$ terms along with their Hermitian conjugate (H.c.) contribute predominantly to the above quantities. The term representing OR_{2a} accounts for the core-polarization effects to all orders, while the OT_1 term represents the extra core-valence correlation effects that were accounted for in the calculations of the ground states of the corresponding Ni-like ions from which atomic states of the Co-like ions were derived. The other two nonlinear terms, $R_{2a}^\dagger OR_{2a}$ and $R_{2a}^\dagger OT_2$, are responsible for including higher-order core-polarization effects in our calculations. It can be seen from Fig. 1 that the most dominating term is the core-polarization term OR_{2a} for all the atomic states that further show an increasing trend with atomic number. As expected, the effect of the core-polarization for the outermost d orbitals are comparatively quite smaller than the inner valence p orbitals, so the contribution to the A_{hf}/g_I values are quite large for the $3p^5 3d^{10} 2P_{1/2,3/2}$ excited states. The next dominating contribution comes from the nonlinear term $R_{2a}^\dagger OR_{2a}$ although the magnitude is smaller compared with the core-polarization effect except for the ground states with $Z = 39, 40, \text{ and } 41$. The other nonlinear term, $R_{2a}^\dagger OT_2$, also contributes significantly, however, the values show an opposite behavior (i.e., negative value) compared with the other three terms. Finally, the core-valence correlation effects through OT_1 seem to give non-negligible contribution to A_{hf}/g_I .

We now would like to discuss the behavior of the above dominating terms for the calculations of B_{hf}/Q_I and the con-

tributions from the above RCC terms to this quantity are plotted in Fig. 2. The behavior for the core-polarization effect in determining the B_{hf}/Q_I values are found to be quite similar to that of A_{hf}/g_I for the excited state $3p^5 3d^{10} 2P_{3/2}$ although they differ in the magnitudes percentage-wise. In contrast, for the ground-state doublets, the core-polarization trend shows an opposite behavior as compared with the A_{hf}/g_I values for the excited states. In fact, it shows an increasing trend in the negative direction with respect to the atomic number. The next leading-order contributions to B_{hf}/Q_I are given by the $R_{2a}^\dagger OR_{2a}$ term, which further shows that, for the state $3p^5 3d^{10} 2P_{3/2}$, their magnitudes are nearly equal for all the investigated ions. On contrary, for the ground-state doublets, the corresponding values are slowly increasing as a function of Z . There are also finite contributions coming from the nonlinear term $R_{2a}^\dagger OT_2$ that show an almost constant trend in the respective states with the increase in atomic number. The core-valence term OT_1 also gives non-negligible contributions to the B_{hf}/Q_I values for all the states.

As mentioned earlier, the quantities of experimental interest are the A_{hf} and B_{hf} values. To obtain these values from our calculations of A_{hf}/g_I and B_{hf}/Q_I , we used the nuclear moments that are listed in the nuclear data table [49] for the most stable isotopes. We have given the final A_{hf} and B_{hf} values for all the four calculated states by combining our RCCSD values of atomic calculations and nuclear moments in Table V. Due to the fact that $I = 1/2$, the B_{hf} values do not exist for Y^{12+} , Rh^{18+} , Ag^{20+} , and Cd^{21+} . The nuclear moments for the stable isotopes for which we have determined the hyperfine structure constants are also listed in the above table. It can be seen that the μ_I values are known very precisely for these isotopes, but many different Q_I values are reported for a few isotopes; especially for $^{91}Zr^{13+}$ and $^{97}Mo^{15+}$. So we suggest that, if the B_{hf} of either of the $3p^6 3d^9 2D_{5/2}$, $3p^6 3d^9 2D_{3/2}$, or $3p^5 3d^{10} 2P_{3/2}$ state is measured precisely for the above

TABLE V. The estimated values of A_{hf} and B_{hf} for the calculated states of the Co-like ions using the RCCSD method. The nuclear parameters for the stable isotopes used to estimate these values are taken from Ref. [49] and they are listed here. As can be seen, the reported Q_I values of the $^{91}\text{Zr}^{13+}$ and $^{97}\text{Mo}^{15+}$ isotopes differ significantly from various works, so we present the B_{hf} values for these ions by considering all the reported values of Q_I . We anticipate that the Q_I values of these isotopes can be inferred more reliably by combining our calculations with possible measurements of the B_{hf} values in these ions.

Ion	I	μ_I	g_I	A_{hf} (in MHz)				Q_I (in b)	B_{hf} (in MHz)		
				$^2D_{5/2}$	$^2D_{3/2}$	$^2P_{3/2}$	$^2P_{1/2}$		$^2D_{5/2}$	$^2D_{3/2}$	$^2P_{3/2}$
$^{89}\text{Y}^{12+}$	$\frac{1}{2}$	-0.137 415 4(3)	-0.274 830 8	-756(4)	-1897(10)	-4494(15)	-25 816(20)				
$^{91}\text{Zr}^{13+}$	$\frac{5}{2}$	-1.303 62(2)	-0.521 448	-1617(8)	-4049(13)	-9426(17)	-54 578(22)	-0.176(3)	-1098(15)	-801(10)	-5893(40)
								-0.257(13)	-1604(12)	-1170(20)	-8606(40)
								-0.206(10)	-1285(15)	-938(10)	-6898(60)
$^{93}\text{Nb}^{14+}$	$\frac{9}{2}$	+6.1705(3)	1.371 22	4767(11)	11 920(20)	27 331(25)	159 433(30)	-0.37(2)	-2590(20)	-1893(22)	-13 692(80)
$^{97}\text{Mo}^{15+}$	$\frac{5}{2}$	-0.9335(1)	-0.373 40	-1449(12)	-3618(18)	-8185(20)	-48 139(30)	0.255(13)	1992(20)	1460(30)	10 399(80)
								0.17(4)	1328(15)	973(12)	6932(50)
								0.27(10)	2109(25)	1546(20)	11 011(70)
$^{99}\text{Tc}^{16+}$	$\frac{9}{2}$	+5.6847(4)	1.263 266	5448(30)	13 595(40)	30 374(45)	180 150(50)	-0.129(6)	-1120(22)	-823(15)	-5782(40)
$^{101}\text{Ru}^{17+}$	$\frac{5}{2}$	-0.719(6)	-0.287 60	-1373(12)	-3425(20)	-7566(40)	-45 290(50)	0.46(2)	4424(40)	3257(30)	22 605(90)
$^{103}\text{Rh}^{18+}$	$\frac{1}{2}$	-0.8840(2)	-1.7680	-9312(40)	-23 219(50)	-50 779(60)	-306 730(80)				
$^{105}\text{Pd}^{19+}$	$\frac{5}{2}$	-0.642(3)	-0.256 80	-1487(20)	-3708(40)	-8034(50)	-489 90(60)	0.660(11)	7703(40)	5701(35)	38 715(90)
								0.65(3)	7587(60)	5615(50)	38 129(80)
$^{109}\text{Ag}^{20+}$	$\frac{1}{2}$	-0.130 690 6(2)	-0.261 381 2	-1659(30)	-4138(40)	-8888(60)	-54 799(80)				
$^{111}\text{Cd}^{21+}$	$\frac{1}{2}$	-0.5948 861(8)	-1.189 772 2	-8258(60)	-20 588(80)	-43 893(90)	-272 786(100)				

ion, then by combining that measured value with our B_{hf}/Q_I calculation it is possible to infer the Q_I value of the respective ion more reliably.

VI. CONCLUSION

We have employed the Fock-space relativistic coupled-cluster method to calculate the atomic wave functions of the first four low-lying $3p^6 3d^9 ^2D_{5/2}$, $3p^6 3d^9 ^2D_{3/2}$, $3p^5 3d^{10} ^2P_{3/2}$, and $3p^5 3d^{10} ^2P_{1/2}$ states of the Co-like ions such as Y^{12+} , Zr^{13+} , Nb^{14+} , Mo^{15+} , Tc^{16+} , Ru^{17+} , Rh^{18+} , Pd^{19+} , Ag^{20+} , and Cd^{21+} , which are one electron less than a closed-shell electronic configuration. The Dirac-Breit interactions along with lower-order QED effects through an effective potential are considered to perform these calculations. Only the dominant singles and doubles excitation configurations were taken into account in our method, and the uncertainties were estimated by analyzing leading-order contributions from the valence triple excitations and truncated basis functions. The ionization potentials of the Ni-like ions of the above elements were first determined in order to obtain the considered atomic states of Co-like ions, and taking their differences the excitation energies of the respective Co-like ions were estimated. Furthermore, the calculated wave functions were used to de-

termine the $E1$, $E2$, and $M1$ transition matrix elements among the aforementioned states of the Co-like ions. Furthermore, using these matrix elements we determine other transition properties such as the line strengths, oscillator strengths, and transition probabilities. The lifetimes of the excited states were estimated from the total transition probabilities from a given excited state and they are compared with the available theoretical values. In addition, we have also determined the magnetic-dipole and electric-quadrupole hyperfine structure constants of the above states of the stable isotopes of Co-like ions. Since the nuclear quadrupole moment of the ^{91}Zr and ^{97}Mo isotopes are not known precisely, we suggest to infer their values by combining our calculations of B_{hf}/Q_I of one of its states with the measurement of B_{hf} of the corresponding state in the future.

ACKNOWLEDGMENTS

D.K.N. gratefully acknowledges the funding support by the Institute for Basic Science in Korea (Grant No. IBS-R024-D1). D.K.N. also acknowledges use of the high performance computing facility (FERMI cluster) at IBS-PCS and B.K.S. acknowledges use of Vikram-100 HPC facility for performing calculations and implementation of the program.

- [1] T. Pütterich, R. Neu, C. Biedermann, R. Radtke, and A. U. Team, *J. Phys. B: At., Mol. Opt. Phys.* **38**, 3071 (2005).
[2] J. Yanagibayashi, T. Nakano, A. Iwamae, H. Kubo, M. Hasuo, and K. Itami, *J. Phys. B: At., Mol. Opt. Phys.* **43**, 144013 (2010).

- [3] S. Sudkewer, *Phys. Scr.* **23**, 72 (1981).
[4] S. Suckewer and E. Hinnov, *Phys. Rev. A* **20**, 578 (1979).
[5] E. Biémont and C. J. Zeippen, *Phys. Scr.* **T65**, 192 (1996).
[6] S. B. Utter, P. Beiersdorfer, and G. V. Brown, *Phys. Rev. A* **61**, 030503(R) (2000).

- [7] J. V. Porto, I. Kink, and J. D. Gillaspay, *Phys. Rev. A* **61**, 054501 (2000).
- [8] Y. Ralchenko, J. N. Tan, J. D. Gillaspay, J. M. Pomeroy, and E. Silver, *Phys. Rev. A* **74**, 042514 (2006).
- [9] J. D. Gillaspay, I. N. Draganić, Y. Ralchenko, J. Reader, J. N. Tan, J. M. Pomeroy, and S. M. Brewer, *Phys. Rev. A* **80**, 010501(R) (2009).
- [10] C. S. Harte *et al.*, *J. Phys. B: At., Mol. Opt. Phys.* **43**, 205004 (2010).
- [11] D. K. Nandy and B. K. Sahoo, *Phys. Rev. A* **94**, 032504 (2016).
- [12] Y.-m. Yu and B. K. Sahoo, *Phys. Rev. A* **99**, 022513 (2019).
- [13] Y.-m. Yu and B. K. Sahoo, *Phys. Rev. A* **97**, 041403(R) (2018).
- [14] Y.-m. Yu and B. K. Sahoo, *Phys. Rev. A* **94**, 062502 (2016).
- [15] M. S. Safronova, V. A. Dzuba, V. V. Flambaum, U. I. Safronova, S. G. Porsev, and M. G. Kozlov, *Phys. Rev. A* **90**, 042513 (2014).
- [16] J. C. Berengut, V. A. Dzuba, V. V. Flambaum, and A. Ong, *Phys. Rev. A* **86**, 022517 (2012).
- [17] V. A. Dzuba and V. V. Flambaum, in *TCP 2014*, edited by M. Wada, P. Schury, and Y. Ichikawa (Springer International Publishing, Cham, 2017), pp. 79–86.
- [18] J. C. Berengut, V. A. Dzuba, and V. V. Flambaum, *Phys. Rev. Lett.* **105**, 120801 (2010).
- [19] U. Feldman, P. Indelicato, and J. Sugar, *J. Opt. Soc. Am. B* **8**, 3 (1991).
- [20] D. K. Nandy and B. K. Sahoo, *Phys. Rev. A* **88**, 052512 (2013).
- [21] D. K. Nandy and B. K. Sahoo, *Astron. Astrophys.* **563**, A25 (2014).
- [22] D. K. Nandy, *Phys. Rev. A* **94**, 052507 (2016).
- [23] C. Cheung, M. S. Safronova, S. G. Porsev, M. G. Kozlov, I. I. Tupitsyn, and A. I. Bondarev, *Phys. Rev. Lett.* **124**, 163001 (2020).
- [24] Y. Ralchenko, I. N. Draganić, D. Osin, J. D. Gillaspay, and J. Reader, *Phys. Rev. A* **83**, 032517 (2011).
- [25] X.-B. Ding, F. Koike, I. Murakami, D. Kato, H. A. Sakaue, C.-Z. Dong, and N. Nakamura, *J. Phys. B: At., Mol. Opt. Phys.* **45**, 035003 (2012).
- [26] S. Suckewer, E. Hinnov, S. Cohen, M. Finkenthal, and K. Sato, *Phys. Rev. A* **26**, 1161 (1982).
- [27] M. H. Prior, *J. Opt. Soc. Am. B* **4**, 144 (1987).
- [28] B. Edlén, *Phys. Scr.* **T8**, 5 (1984).
- [29] J. O. Ekberg, U. Feldman, J. F. Seely, C. M. Brown, J. Reader, and N. Acquista, *J. Opt. Soc. Am. B* **4**, 1913 (1987).
- [30] E. Alexander, M. Even-Zohar, B. S. Fraenkel, and S. Goldsmith, *J. Opt. Soc. Am.* **61**, 508 (1971).
- [31] P. Burkhalter, J. Reader, and R. D. Cowan, *J. Opt. Soc. Am.* **70**, 912 (1980).
- [32] X. L. Guo, R. Si, S. Li, M. Huang, R. Hutton, Y. S. Wang, C. Y. Chen, Y. M. Zou, K. Wang, J. Yan, C. Y. Li, and T. Brage, *Phys. Rev. A* **93**, 012513 (2016).
- [33] I. Grant, B. McKenzie, P. Norrington, D. Mayers, and N. Pyper, *Comput. Phys. Commun.* **21**, 207 (1980).
- [34] A. Kramida, Yu. Ralchenko, J. Reader, and NIST ASD Team, NIST Atomic Spectra Database (ver. 5.8). Available at <https://physics.nist.gov/asd> [2021, August 12]. National Institute of Standards and Technology, Gaithersburg, MD (2020).
- [35] I. P. Grant, *Relativistic Quantum Theory of Atoms and Molecules* (Springer, New York, 2007).
- [36] J. S. M. Ginges and J. C. Berengut, *Phys. Rev. A* **93**, 052509 (2016).
- [37] I. Lindgren and J. Morrison, *Atomic Many-Body Theory* (Springer-Verlag, Berlin, 1986).
- [38] M. Reiher and A. Wolf, *Relativistic Quantum Chemistry: The Fundamental Theory of Molecular Science* (Wiley-VCH Verlag, Weinheim, Germany, 2014).
- [39] W. R. Johnson, *Atomic Structure Theory* (Springer-Verlag, Berlin, 2007).
- [40] I. Shavitt and R. J. Bartlett, *Many-Body Methods in Chemistry and Physics: MBPT and Coupled-Cluster Theory* (Cambridge University Press, Cambridge, 2009).
- [41] B. K. Sahoo, S. Majumder, R. K. Chaudhuri, B. P. Das, and D. Mukherjee, *J. Phys. B: At., Mol. Opt. Phys.* **37**, 3409 (2004).
- [42] A. N. Ryabtsev and J. Reader, *J. Opt. Soc. Am.* **72**, 710 (1982).
- [43] D. K. Nandy and B. K. Sahoo, *Phys. Rev. A* **90**, 050503(R) (2014).
- [44] A. Glushkov and L. Ivanov, *Phys. Lett. A* **170**, 33 (1992).
- [45] M. Kaur, D. F. Dar, B. Sahoo, and B. Arora, *At. Data Nucl. Data Tables* **137**, 101381 (2021).
- [46] A. Mohanty and E. Clementi, *Modern Techniques in Computational Chemistry: MOTECC-89* (Springer, Netherlands, 1989), Chap. 4, p. 169.
- [47] I. I. Sobelman, *Atomic Spectra and Radiative Transitions* (Springer-Verlag, Berlin, 1979).
- [48] C. Schwartz, *Phys. Rev.* **97**, 380 (1955).
- [49] N. Stone, *At. Data Nucl. Data Tables* **90**, 75 (2005).